

# A Statistical Evaluation of Coherence Time for Non-Terrestrial Communications

Pinjun Zheng, *Graduate Student Member, IEEE*, Tareq Y. Al-Naffouri, *Senior Member, IEEE*

**Abstract**—Non-terrestrial networks (NTNs) are recognized as essential components of the next-generation communication systems. This letter evaluates the coherence time for non-terrestrial channels, revealing that the rapid mobility of non-terrestrial base stations (BSs) substantially diminishes channel coherence time. Our results demonstrate that the existence and enhancement of the line-of-sight channel play a crucial role in extending coherence time. Furthermore, unlike terrestrial networks, adjustments to receiver beamwidth seldom affect coherence time with a high-speed motion of the BS in NTNs.

**Index Terms**—Coherence time, non-terrestrial communication, NTN, LEO satellite, autocorrelation, von-Mises-Fisher distribution.

## I. INTRODUCTION

Serving as potent supplements to terrestrial networks, non-terrestrial base stations (BSs) offer expansive coverage, reduced latency, and enhanced efficiency for wireless communication, sensing, and localization services [1]–[3]. Like terrestrial networks, non-terrestrial communication greatly benefits from multiple-input multiple-output (MIMO) systems and beamforming techniques [4]. However, the coherence time of air-to-ground channels arises as a critical concern, as it governs the frequency at which precoders and combiners must be updated. To the best of the authors' knowledge, this issue has not yet been well investigated in the literature.

The channel coherence time refers to the duration after which the channel loses its correlation. Typically, the channel coherence time  $T_c$  is approximately the inverse of the Doppler spread  $f_D$ , i.e.,  $T_c \simeq 1/f_D$  [5]. Non-terrestrial BSs such as LEO satellites generally experience high-speed mobility, thus inducing significant Doppler frequency shifts in received signals [1], [3]. Such an increase in Doppler frequency diminishes the channel coherence time and in turn, increases the pilot overhead. Apart from that, the coherence time is also related to the beamwidth at the receiver. A narrower beamwidth aids in mitigating destructive multipath components while concurrently accentuating the effect of misalignment. Notably, the results in [6] and [7] reveal that by carefully designing beamwidth, the coherence time can be effectively enlarged. Nonetheless, all these aforementioned results are based on the terrestrial network without accounting for the mobility of the BS, which might not be applicable to non-terrestrial networks. To offer a more accurate and comprehensive assessment of

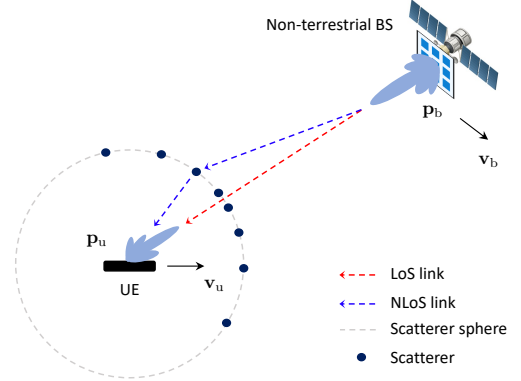


Fig. 1. Illustration of a downlink communication from a mobile non-terrestrial BS to a mobile UE on the ground. Both LoS and NLoS links exist and the scatterers are assumed to be distributed on a sphere.

coherence time in air-to-ground channels, this letter extends the analysis in [7] by (i) integrating dual-mobility at both transmitter and receiver ends, (ii) employing a 3D geometric model instead of 2D, and (iii) utilizing accurate calculation of the Doppler phase shift in integral form  $\phi_D(t) = \int_0^t f_D(\tau) d\tau$  instead of the approximate linear form  $\phi_D(t) = f_D(0)t$ .

## II. SYSTEM AND CHANNEL MODEL

We consider a wireless communication system featuring a moving non-terrestrial BS and a moving UE on the ground, as illustrated in Fig. 1. Let  $\mathbf{p}_b$ ,  $\mathbf{v}_b$ ,  $\mathbf{p}_u$ ,  $\mathbf{v}_u \in \mathbb{R}^3$  denote the BS's position, BS's velocity, UE's position, and UE's velocity, respectively. We assume that velocities  $\mathbf{v}_b$  and  $\mathbf{v}_u$  are fixed and so positions change linearly with time as  $\mathbf{p}_b(t) = \mathbf{p}_b(0) + \mathbf{v}_b t$  and  $\mathbf{p}_u(t) = \mathbf{p}_u(0) + \mathbf{v}_u t$ . By default, we designate  $\mathbf{p}_u(0)$  as the origin of the coordinate system for all positions. Since a dominant LoS link is crucial for non-terrestrial communications [8], [9], we examine a scenario with a dominant LoS link and multiple NLoS links. Hence, the wireless channel can be expressed as

$$h(t) = \sqrt{\frac{K}{K+1}} h_L(t) + \sqrt{\frac{1}{K+1}} h_N(t), \quad (1)$$

where  $K$  is the Rician factor denoting the ratio between the power of LoS and NLoS signals.

### A. The LoS Channel

The narrowband equivalent lowpass channel impulse response of the LoS path can be written as [5]

$$h_L(t) = \sqrt{G_b(t)G_u(t)} e^{j2\pi(\phi(t) - f_c t)}, \quad (2)$$

The authors are with the Electrical and Computer Engineering Program, Division of Computer, Electrical and Mathematical Sciences and Engineering (CEMSE), King Abdullah University of Science and Technology (KAUST), Thuwal, 23955-6900, Kingdom of Saudi Arabia. Email: {pinjun.zheng; tareq.alnaffouri}@kaust.edu.sa.

where  $G_b(t)$  and  $G_u(t)$  respectively denote beam patterns at BS and UE,  $\phi(t)$  is the phase shift due to the Doppler effect,  $f_c$  is the carrier frequency, and  $\xi$  is the channel delay. For both BS and UE, we utilize a simple beam pattern as  $\cos^q(\theta)$  [10], where  $\theta$  denotes the angle between the direction of LoS and the direction of beam major lobe (pointing direction). The power factor  $q$  controls the beam directivity and can be related to the half-power beamwidth (HPBW) (denoted as  $\psi$ ) by  $\psi = 2 \arccos(2^{-1/q})$ . Then, the beam patterns can be expressed as

$$G_b(t) = \left( \frac{(\mathbf{p}_u(t) - \mathbf{p}_b(t))^T \mathbf{b}}{\|\mathbf{p}_u(t) - \mathbf{p}_b(t)\|} \right)^{q_b}, \quad (3)$$

$$G_u(t) = \left( \frac{(\mathbf{p}_b(t) - \mathbf{p}_u(t))^T \mathbf{u}}{\|\mathbf{p}_b(t) - \mathbf{p}_u(t)\|} \right)^{q_u}, \quad (4)$$

where  $\mathbf{b} \in \mathbb{R}^3$  and  $\mathbf{u} \in \mathbb{R}^3$  respectively denote the unit directional vectors of the major lobes at BS and UE, and  $q_b$  and  $q_u$  respectively stand for the directivity of the beams at the BS and UE. Here, the dependence of the beam pattern on time  $t$  signifies the beam misalignment. Since the Doppler frequency at time  $t$  is given by  $f_D(t) = \frac{(\mathbf{v}_u - \mathbf{v}_b)^T (\mathbf{p}_b(t) - \mathbf{p}_u(t))}{\lambda \|\mathbf{p}_b(t) - \mathbf{p}_u(t)\|}$  [5], the Doppler shift  $\phi(t)$  can be obtained as

$$\begin{aligned} \phi(t) &= \int_0^t \frac{(\mathbf{v}_u - \mathbf{v}_b)^T (\mathbf{p}_b(\tau) - \mathbf{p}_u(\tau))}{\lambda \|\mathbf{p}_b(\tau) - \mathbf{p}_u(\tau)\|} d\tau, \\ &= -\frac{1}{\lambda} \int_0^t \frac{\mathbf{v}^T (\mathbf{p}_0 + \mathbf{v}\tau)}{\|\mathbf{p}_0 + \mathbf{v}\tau\|} d\tau = -\frac{1}{\lambda} (\|\mathbf{p}_0 + \mathbf{v}t\| - \|\mathbf{p}_0\|), \end{aligned} \quad (5)$$

where  $\mathbf{p}_0 = \mathbf{p}_b(0) - \mathbf{p}_u(0)$  and  $\mathbf{v} = \mathbf{v}_b - \mathbf{v}_u$ .

### B. The NLoS Channel

Analogous to [7], we assume that the scatterers are distributed on a 3D sphere  $\mathbb{S}^2$  with radius  $R$  centered around the UE, and that the reflected signals are uncorrelated with each other (known as the uncorrelated scattering (US) assumption [5]). Then, the NLoS channel impulse response can be characterized as [6], [7]

$$h_N(t) = \int_{\mathbb{S}^2} \sqrt{p(\Omega) G_b(t, \Omega) G_u(t, \Omega)} e^{j2\pi(\varphi(t, \Omega) + \gamma(\Omega) - f_c \zeta(\Omega))} d\Omega,$$

where  $p(\Omega)$  is the probability density function (PDF) of the scatterers' distribution on the sphere,  $\varphi(t, \Omega)$  is the Doppler shift in NLoS links,  $\gamma(\Omega) \sim U[0, 1]$  is a uniformly distributed random phase shift associated with each scatterer, and  $\zeta(\Omega)$  denotes the NLoS channel delays. Here,  $\mathbb{S}^2 \subset \mathbb{R}^3$  represents the considered 3D sphere and  $\Omega$  is the solid angle corresponding to an infinitesimal area on the sphere. Typically, each solid angle  $\Omega$  can be uniquely characterized using an azimuth angle  $\theta_{az}$  and an elevation angle  $\theta_{el}$ , i.e.,  $\Omega = \{\theta_{az}, \theta_{el}\}$ , as shown in Fig. 2-(a). The term  $p(\Omega) G_b(t, \Omega) G_u(t, \Omega)$  is also known as the effective power angular spectrum [6].

In this work, we adopt the 3D von-Mises-Fisher (vMF) distribution to describe the distribution of scatterers over the sphere. Specifically, a 3D vMF distribution has the PDF [11]

$$p(\Omega; \boldsymbol{\mu}, \rho) = \frac{\rho e^{\rho \boldsymbol{\mu}^T \mathbf{n}(\Omega)}}{2\pi(e^\rho - e^{-\rho})}, \quad (6)$$

where  $\boldsymbol{\mu} \in \mathbb{R}^3$  is a unit-norm vector indicating the mean direction,  $\rho > 0$  is the concentration parameter, and  $\mathbf{n}(\Omega)$

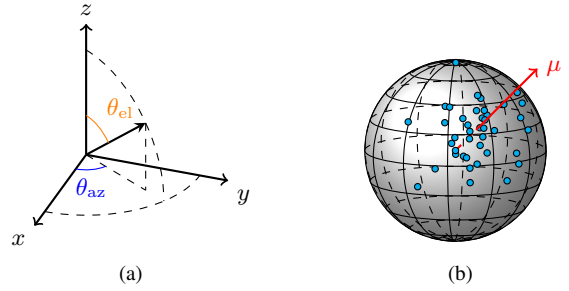


Fig. 2. Geometric setups. (a) The definition of the azimuth and elevation components of a solid angle. (b) A realization of random scatterers conformed to 3D vMF distribution.

is the directional vector corresponding to the solid angle  $\Omega$ , i.e.,  $\mathbf{n}(\Omega) = [\cos(\theta_{az}) \sin(\theta_{el}), \sin(\theta_{az}) \sin(\theta_{el}), \cos(\theta_{el})]^T$ . A higher value of  $\rho$  indicates that the scatterers are more concentrated around the mean direction  $\boldsymbol{\mu}$ . Fig. 2-(b) visualizes a realization of a set of vMF-distributed scatterers on a sphere.

The beam patterns  $G_b(t, \Omega)$  and  $G_u(t, \Omega)$  can be obtained according to (3) and (4) by replacing  $\mathbf{p}_u(t)$  and  $\mathbf{p}_b(t)$  with  $\mathbf{p}(\Omega) = R\mathbf{n}(\Omega)$ . Since the Doppler frequency of the NLoS signal corresponding to the solid angle  $\Omega$  is given by  $f_D(t, \Omega) = \frac{\mathbf{v}_b^T (\mathbf{p}(\Omega) - \mathbf{p}_b(t))}{\lambda \|\mathbf{p}(\Omega) - \mathbf{p}_b(t)\|} + \frac{\mathbf{v}_u^T (\mathbf{p}(\Omega) - \mathbf{p}_u(t))}{\lambda \|\mathbf{p}(\Omega) - \mathbf{p}_u(t)\|}$ , the Doppler shift  $\varphi(t, \Omega)$  can be obtained as

$$\begin{aligned} \varphi(t, \Omega) &= \int_0^t \frac{\mathbf{v}_b^T (\mathbf{r}(\Omega) - \mathbf{v}_b\tau)}{\lambda \|\mathbf{r}(\Omega) - \mathbf{v}_b\tau\|} d\tau + \int_0^t \frac{\mathbf{v}_u^T (\mathbf{s}(\Omega) - \mathbf{v}_u\tau)}{\lambda \|\mathbf{s}(\Omega) - \mathbf{v}_u\tau\|} d\tau, \\ &= -\frac{1}{\lambda} (\|\mathbf{r}(\Omega) - \mathbf{v}_b t\| - \|\mathbf{r}(\Omega)\| + \|\mathbf{s}(\Omega) - \mathbf{v}_u t\| - \|\mathbf{s}(\Omega)\|), \end{aligned} \quad (7)$$

where  $\mathbf{r}(\Omega) = \mathbf{p}(\Omega) - \mathbf{p}_b(0)$  and  $\mathbf{s}(\Omega) = \mathbf{p}(\Omega) - \mathbf{p}_u(0)$ .

### III. CHANNEL AUTOCORRELATION AND COHERENCE TIME DERIVATION

The channel coherence time  $T_c$  is defined as a time after which the channel autocorrelation decreases to a predefined threshold  $\epsilon$  [5]–[7]. The channel decorrelation results from two effects: (i) The superimposed distortion effect of Doppler shifts and random phases caused by different multipath scatterers and (ii) the beam misalignment due to the BS's and/or UE's movements. The model presented in Section II has taken these two effects into account.

Although NLoS channels are commonly assumed as wide-sense stationary [5], this assumption does not hold for the LoS channel. Therefore, we keep the time variable  $t$  and write the channel autocorrelation as

$$\begin{aligned} A_h(t, \tau) &= \mathbb{E}[h(t)h^*(t + \tau)], \\ &= \frac{K}{K+1} \mathbb{E}[h_L(t)h_L^*(t + \tau)] + \frac{\sqrt{K}}{K+1} \mathbb{E}[h_L(t)h_N^*(t + \tau)] \\ &\quad + \frac{\sqrt{K}}{K+1} \mathbb{E}[h_N(t)h_L^*(t + \tau)] + \frac{1}{K+1} \mathbb{E}[h_N(t)h_N^*(t + \tau)]. \end{aligned} \quad (8)$$

Then, these four terms are derived individually in (11)–(14). Note that the LoS channel  $h_L(t)$  is a deterministic function of  $t$  while the NLoS channel  $h_N(t)$  is a stochastic process. Step (a) in (12) and step (b) in (13) follows from that  $\gamma(\Omega) \sim U[0, 1]$ , thus  $\mathbb{E}[e^{-j2\pi\gamma(\Omega)}] = 0$  and so  $\mathbb{E}[h_N(t)] = \int_{\mathbb{S}^2} \sqrt{p(\Omega) G_b(t, \Omega) G_u(t, \Omega)} e^{j2\pi(\varphi(t, \Omega) - f_c \zeta(\Omega))} \mathbb{E}[e^{j2\pi\gamma(\Omega)}] d\Omega = 0$ .

$$\mathbb{E}[h_L(t)h_L^*(t+\tau)] = \sqrt{G_b(t)G_b(t+\tau)G_u(t)G_u(t+\tau)}e^{j2\pi(\phi(t)-\phi(t+\tau))}, \quad (11)$$

$$\mathbb{E}[h_L(t)h_N^*(t+\tau)] = h_L(t)\mathbb{E}[h_N^*(t+\tau)] \stackrel{(a)}{=} 0, \quad (12)$$

$$\mathbb{E}[h_N(t)h_L^*(t+\tau)] = h_L^*(t+\tau)\mathbb{E}[h_N(t)] \stackrel{(b)}{=} 0, \quad (13)$$

$$\begin{aligned} & \mathbb{E}[h_N(t)h_N^*(t+\tau)] \\ &= \mathbb{E}\left[\int_{\mathbb{S}^2}\int_{\mathbb{S}^2}\sqrt{p(\Omega_1)p(\Omega_2)G_b(t,\Omega_1)G_b(t+\tau,\Omega_2)G_u(t,\Omega_1)G_u(t+\tau,\Omega_2)}e^{j2\pi(\varphi(t,\Omega_1)-\varphi(t+\tau,\Omega_2))}e^{j2\pi(\gamma(\Omega_1)-\gamma(\Omega_2))}e^{j2\pi f_c(\zeta(\Omega_2)-\zeta(\Omega_1))}d\Omega_1d\Omega_2\right], \\ &= \int_{\mathbb{S}^2}\int_{\mathbb{S}^2}\sqrt{p(\Omega_1)p(\Omega_2)G_b(t,\Omega_1)G_b(t+\tau,\Omega_2)G_u(t,\Omega_1)G_u(t+\tau,\Omega_2)}e^{j2\pi(\varphi(t,\Omega_1)-\varphi(t+\tau,\Omega_2))}\mathbb{E}\left[e^{j2\pi(\gamma(\Omega_1)-\gamma(\Omega_2))}\right]e^{j2\pi f_c(\zeta(\Omega_2)-\zeta(\Omega_1))}d\Omega_1d\Omega_2, \\ &\stackrel{(c)}{=} \int_{\mathbb{S}^2}\sqrt{p^2(\Omega)G_b(t,\Omega)G_b(t+\tau,\Omega)G_u(t,\Omega)G_u(t+\tau,\Omega)}e^{j2\pi(\varphi(t,\Omega)-\varphi(t+\tau,\Omega))}d\Omega. \end{aligned} \quad (14)$$

Moreover, step (c) in (14) follows from the US assumption. Specifically, since the random phase shifts caused by different scatterers are uncorrelated, we have

$$\begin{aligned} & \mathbb{E}\left[e^{j2\pi(\gamma(\Omega_1)-\gamma(\Omega_2))}\right] \\ &= \begin{cases} \mathbb{E}\left[e^{j2\pi(\gamma(\Omega_1))}\right]\mathbb{E}\left[e^{-j2\pi(\gamma(\Omega_2))}\right] = 0, & \text{if } \Omega_1 \neq \Omega_2, \\ 1, & \text{if } \Omega_1 = \Omega_2, \end{cases} \end{aligned} \quad (9)$$

from which (14) follows. It is not possible to further simplify (14), but we can evaluate it numerically. Specifically, the integral over  $\mathbb{S}^2$  can be implemented by integrating the objective function over the azimuth and elevation components [10]

$$\int_{\mathbb{S}^2} f(\Omega)d\Omega = \int_0^{2\pi} \int_0^\pi f(\theta_{az}, \theta_{el}) \sin(\theta_{el})d\theta_{el}d\theta_{az}. \quad (10)$$

A normalization step is further performed to  $\bar{A}_h(t, \tau)$ , so that we obtain  $\bar{A}_h(t, \tau) = A_h(t, \tau)/A_h(t, 0)$ . Subsequently, we can define the channel coherence time  $T_c$  as

$$T_c(t) = \min \{ \tau \mid |\bar{A}_h(t, \tau)| < \epsilon \}, \quad 0 < \epsilon < 1. \quad (15)$$

Here, the coherence time  $T_c$  is a function of  $t$  since the LoS channel is not statistically stationary.

#### IV. NUMERICAL RESULTS

This section conducts numerical simulations. As an example, the BS is assumed to be deployed in a low Earth orbit (LEO) satellite [12], performing downlink communications to a ground user at a carrier frequency  $f_c = 28$  GHz. By default, we set  $\mathbf{p}_b(0) = [-1, 0, 500]^T$  km,  $\mathbf{v}_b = [7, 0, 0]^T$  km/s,  $\mathbf{p}_u(0) = [0, 0, 0]^T$  m,  $\mathbf{v}_u = [0, 2, 0]^T$  m/s. The radius of the scatterer sphere is set as  $R = 1000\lambda$ , where  $\lambda$  denotes the signal wavelength. We set the concentration of the scatterers as  $\rho = 30$ , and the mean direction  $\boldsymbol{\mu}$  as the LoS direction at  $t = 0$ . Additionally, the HPBWs  $\psi$  at the BS and UE are  $2^\circ$  and  $20^\circ$ , respectively. In the evaluations of the autocorrelation  $\bar{A}_h(t, \tau)$ , we pick  $t = 0$  thus observing over  $\tau$  to determine the coherence time  $T_c(0)$  according to (15).

Fig. 3 plots  $|\bar{A}_h(0, \tau)|$  vs.  $\tau$  across different Rician factor  $K$ . Observe that a stronger LoS component (higher  $K$ ) can effectively delay the decorrelation of the channel. In particular, the coherence time of the LoS component ( $K = +\infty$ ) can be significantly longer than that of the NLoS component ( $K = 0$ ) by up to six orders of magnitude. This underscores the paramount importance of the LoS channel in non-terrestrial communications. For cases  $0 < K < +\infty$  where both the

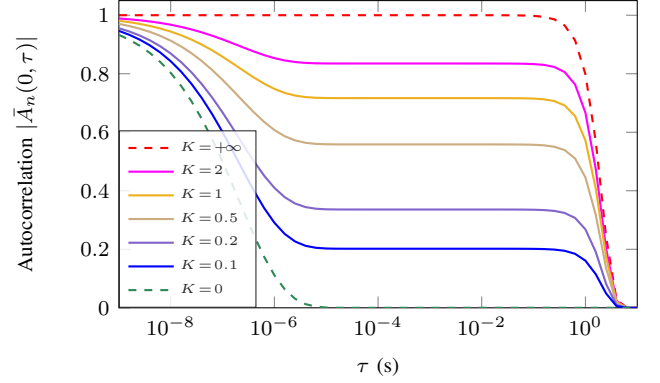


Fig. 3. The evaluation of  $|\bar{A}_h(0, \tau)|$  vs.  $\tau$  over Rician factor  $K = \{0, 0.1, 0.2, 0.5, 1, 2, +\infty\}$ , where  $K = 0$  and  $K = +\infty$  correspond to the NLoS-only and LoS-only cases, respectively.

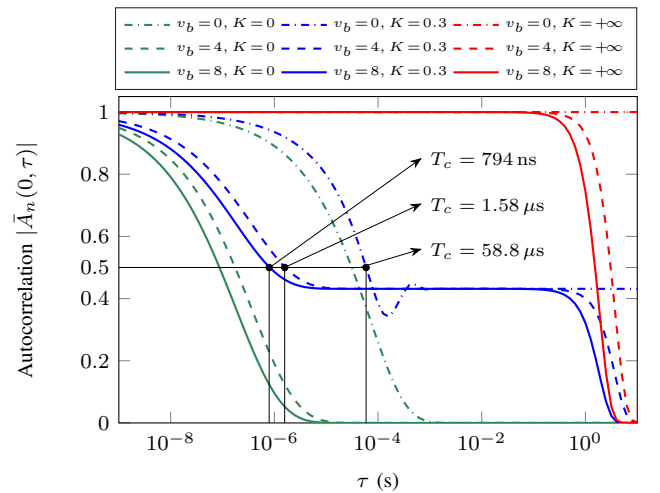


Fig. 4. The evaluation of  $|\bar{A}_h(0, \tau)|$  vs.  $\tau$  with different speeds of the BS. We set  $\mathbf{v}_b = [v_b, 0, 0]^T$  and test over  $v_b = \{0, 4, 8\}$  km/s. The evaluation is also performed over  $K = \{0, 0.3, +\infty\}$ .

LoS and NLoS components exist, the channel autocorrelation initially decreases with the NLoS component, then stabilizes after the NLoS component decorrelates to zero, and eventually diminishes to zero with the LoS component. During this process, a higher  $K$  value can aid in the preservation of channel correlation, thus sustaining the stable stage at a higher autocorrelation level.

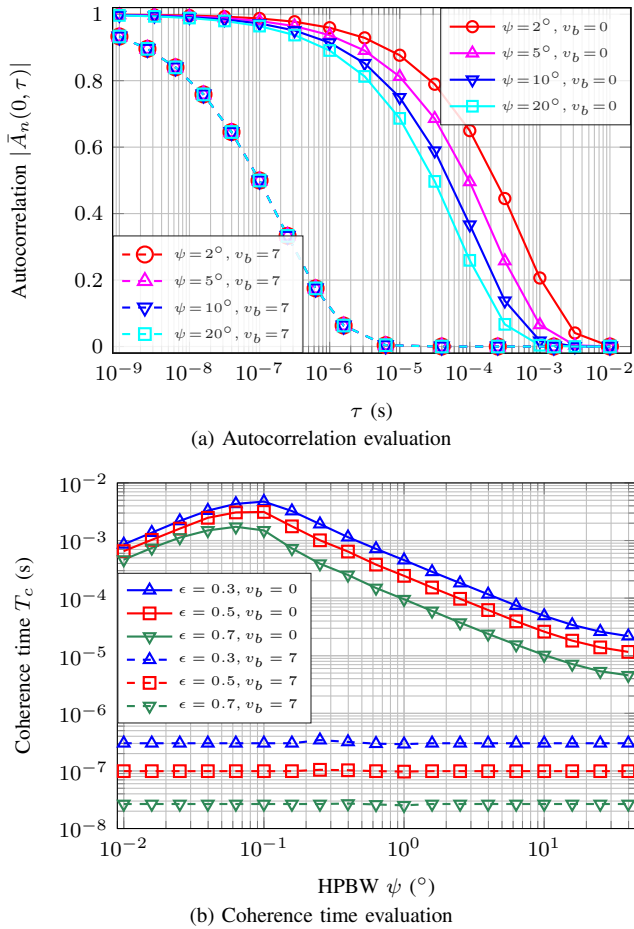


Fig. 5. The evaluation of channel autocorrelation and coherence time across various receiver beamwidths.

To investigate the impact of the BS's mobility, Fig. 4 illustrates  $|\bar{A}_h(0, \tau)|$  vs.  $\tau$  when the LEO satellite moves with different speeds  $v_b = \{0, 4, 8\}$  km/s with  $\mathbf{v}_b = [v_b, 0, 0]^T$ . Benchmarked against the  $v_b = 0$  case, the mobility of the LEO satellite substantially accelerates the channel decorrelation and thus reduces the coherence time. Fig. 4 shows an example with  $\epsilon = 0.5$  and  $K = 0.3$ . When  $v_b = 0$ , the coherence time  $T_c$  is approximately  $58.8 \mu\text{s}$ , which is aligned with the results in [6], [7]. However, when we enlarge the BS's speed to 4 km/s and 8 km/s,<sup>1</sup> the coherence times are reduced to  $1.58 \mu\text{s}$  and  $0.794 \mu\text{s}$ , respectively. This reveals that a high-speed moving BS would result in a significant reduction in coherence time, which can even make beamforming impossible considering a typical mmWave OFDM symbol duration of several microseconds [13]. Based on Fig. 3 and Fig. 4, enhancing the LoS link could be an effective solution.

As outlined in [6] and [7], for terrestrial mmWave networks, adjusting receiver beamwidth is an effective strategy to combat the coherence time reduction. We now revisit this issue in the context of non-terrestrial networks. Following [7], here we

<sup>1</sup>The typical orbit speed of LEO satellites is 5–10 km/s [12]. However, the velocity  $\mathbf{v}_b$  defined in this letter is the relative velocity of the satellite w.r.t. the ground user. Determining it requires further consideration of the Earth's rotation, which can vary depending on the satellite orbit and position.

test a scenario where the LoS channel is absent. Fig. 5-(a) depicts  $|\bar{A}_h(0, \tau)|$  over different HPBW  $\psi$  at the UE. When the BS remains static (solid curves), the channel autocorrelation varies with  $\psi$ . However, with the BS in motion (dashed curves), adjusting  $\psi$  no longer impacts the autocorrelation, as these curves coincide. Fig. 5-(b) provides a more intuitive evaluation showing the relationship between coherence time  $T_c$  and receiver HPBW  $\psi$ . For static BS, there exists an optimal beamwidth  $\psi$  that maximizes  $T_c$ , consistent with findings in [6] and [7]. However, with a 7 km/s velocity of the BS, channel coherence times decrease to extremely low levels and remain constant across different  $\psi$  values. This suggests that optimizing receiver beamwidth no longer extends channel coherence time. These results again unveil that non-terrestrial communications may be infeasible without a LoS link, not only due to weak signal reception but also because of the extremely short channel coherence time.

## V. CONCLUSION

This letter studies the coherence time of air-to-ground channels through a statistical analysis of channel autocorrelation. Our analysis reveals that the mobility of the BS significantly diminishes channel coherence time, while enhancing the LoS channel can effectively mitigate this effect. These results underscore, once more, the essential role of the LoS channel in non-terrestrial communications from a channel coherence time perspective.

## REFERENCES

- [1] 3GPP TR 38.821 v16.2.0, "Solutions for NR to support non-terrestrial networks (NTN) (release 16)," *Tech. Rep.*, Mar. 2023.
- [2] M. Giordani and M. Zorzi, "Non-terrestrial networks in the 6G era: Challenges and opportunities," *IEEE Network*, vol. 35, no. 2, pp. 244–251, 2021.
- [3] P. Zheng, X. Liu, J. He, G. Seco-Granados, and T. Y. Al-Naffouri, "LEO satellite and RIS: Two keys to seamless indoor and outdoor localization," *preprint arXiv:2312.16946*, 2023.
- [4] M. Khammassi, A. Kammoun, and M.-S. Alouini, "Precoding for high-throughput satellite communication systems: A survey," *IEEE Communications Surveys & Tutorials*, vol. 26, no. 1, pp. 80–118, 2024.
- [5] A. Goldsmith, *Wireless communications*. Cambridge university press, 2005.
- [6] V. Va and R. W. Heath, "Basic relationship between channel coherence time and beamwidth in vehicular channels," in *IEEE 82nd Vehicular Technology Conference (VTC2015-Fall)*, 2015.
- [7] V. Va, J. Choi, and R. W. Heath, "The impact of beamwidth on temporal channel variation in vehicular channels and its implications," *IEEE Transactions on Vehicular Technology*, vol. 66, no. 6, pp. 5014–5029, 2017.
- [8] 3GPP TR 38.811 v15.4.0, "Study on new radio (NR) to support non-terrestrial networks (release 15)," *Tech. Rep.*, Sept. 2020.
- [9] P. Zheng, X. Liu, and T. Y. Al-Naffouri, "LEO-and RIS-empowered user tracking: A Riemannian manifold approach," *preprint arXiv:2403.05838*, 2024.
- [10] C. A. Balanis, *Antenna theory: analysis and design*. John Wiley & sons, 2016.
- [11] J. Straub, "Bayesian inference with the von-Mises-Fisher distribution in 3D," <http://people.csail.mit.edu/jstraub/download/straub2017vonMisesFisherInference.pdf> (accessed Mar. 27, 2024).
- [12] Y. Su, Y. Liu, Y. Zhou, J. Yuan, H. Cao, and J. Shi, "Broadband LEO satellite communications: Architectures and key technologies," *IEEE Wireless Communications*, vol. 26, no. 2, pp. 55–61, 2019.
- [13] M. Mezzavilla, M. Zhang, M. Polese, R. Ford, S. Dutta, S. Rangan, and M. Zorzi, "End-to-end simulation of 5G mmWave networks," *IEEE Communications Surveys & Tutorials*, vol. 20, no. 3, pp. 2237–2263, 2018.